# Experimental Study and Finite Element Analysis on the Seismic Performance of Ancient Architectural Kanchuang Frame with Different Impact Parameters Considered

Junhong Huan , Ab, Xiaoyi Zhou, Ab Xiaodong Guo, Wei Wang, Donghui Ma, and Yue He

To study the seismic performance of ancient timber structures with attached windows and masonry walls, a low-cycle reciprocating load test was conducted on a 1:2 scaled model of the Kanchuang frame. The frame's failure modes, hysteretic behavior, skeleton curves, stiffness degradation, and energy dissipation capacity of the frame were obtained. Test results showed that the masonry wall of the structure was the first to crack and fail. The tenons of the wood window pulled out of the mortises gradually while the loading displacement increased. In addition, finite element models of the Chinese traditional Kanchuang frame were established and analyzed. The test results were basically consistent with the finite element analysis results. Based on the finite element models, the influences of impact parameters including friction coefficient, elastic modulus, compressive strength in parallel-to-grain directions, and vertical loads on the seismic performance of the Kanchuang frame were analyzed. The results showed that the ultimate load-bearing capacity, initial stiffness, and energy dissipation capacity of the Kanchuang frame are increased with the increase of friction coefficient, compress strength, and the elastic modulus. The influence of elastic modulus in perpendicular-to-grain directions was minor. The initial stiffness and energy dissipation capacity of the structure increased while the vertical loads increased. However, the ultimate peak loads and stiffness decreased with the increase of the vertical loads.

DOI: 10.15376/biores.20.2.4304-4329

Keywords: Ancient architecture; Kanchuang frame; Finite element analysis; Seismic performance; Low-cycle reciprocating test

Contact information: a: School of Civil Engineering, Shijiazhuang Tiedao University, Shijiazhuang 050043, China; b: Key Laboratory of Roads and Railway Engineering Safety Control (Shijiazhuang Tiedao University), Ministry of Education, Shijiazhuang, 050043, China; c: Beijing Engineering Technology Research Center for Historic Building Protection, Beijing University of Technology, Beijing 100124, China; \*Corresponding author: junhong love@126.com

### INTRODUCTION

The Kanchuang frame is a unique feature of Chinese ancient timber structures. It is not only the enclosing part of the entire building but also has functions of transferring inplane and vertical loads, energy dissipation, and seismic reduction. It embodies rich cultural values and is an important component of Chinese ancient timber buildings. The Kanchuang frame is widely used in Chinese ancient buildings, such as the Forbidden City

in Beijing and the Shenyang Imperial Palace, as shown in Fig. 1. However, China is located in a region prone to earthquakes, and many ancient buildings have been damaged and destroyed in previous earthquakes (An *et al.* 2022). Consequently, in recent years, many scholars have conducted research on the seismic performance of ancient timber structures.



Fig. 1. The Wenhua Hall of the Forbidden City

Some research shows that mortise and tenon joints are the key points of ancient timber structures (Sun et al. 2022; An et al. 2024). Consequently, some scholars have conducted experimental studies and finite element analyses on the seismic performance of timber mortise and tenon joints. Xue et al. (2023) studied the seismic performance of fullsize straight tenon joints by finite element numerical simulation, and revealed the effects of elastic modulus, axial load, friction coefficient, and compressive strength in perpendicular-to-grain radial directions on the bending capacity and rotational stiffness of the joints. Hu and Liu (2020) and Zhang and Hu (2021) further investigated the bending capacity and bending stiffness of mortise and tenon joints using finite element methods. Results showed that the width of the tenon significantly affects the bending stiffness. Considering the joint damage caused by long-term loads, natural disasters, and human damages, Ben et al. (2019) established a theoretical model of a Chinese traditional timber frame with straight-tenon connections to explore the impact of damages on the mechanical performance. Bai et al. (2023a,b) and Ma et al. (2023) studied the effects of deformation damage and looseness of mortise and tenon joints on the seismic performance of ancient timber buildings through quasi-static tests, acoustic emission tests, shaking table tests, and finite element numerical simulations in order to improve the load-bearing capacity and stability of tenon and mortise joints in damaged ancient timber structures, thereby enhancing their structural integrity and seismic performance. Some scholars have studied some reinforcement devices and applied them to mortise and tenon joints. Huan et al. (2019) came up with some reinforcement devices that can improve the seismic performance of mortise and tenon joints while preserving the semi-rigid characteristics of the mortise and tenon joints. The test results indicated that the reinforcement devices effectively enhanced the stiffness, peak load-bearing capacity, and energy dissipation ability of the joints. Jin et al. (2022) studied the reinforcement effect of nails, steel plates and wooden strips through quasi-static tests. Zhao et al. (2019) and Yi et al. (2023) studied the enhancement effects on the seismic performance of tenon and mortise joints using

CFRP fabrics and viscous dampers, respectively, all these studies provide references for the reinforcement and restoration of ancient timber structures.

Based on the former studies of mortise and tenon joints, some researchers studied the seismic performance of timber frame with mortise and tenon joints. As a basic structural unit of ancient buildings, the performance of timber frame without any infilled wall or other components (simplified to timber frame) is crucial to the stability and safety of the entire structure (He et al. 2022; Meng et al. 2022). Yang et al. (2024) used finite element numerical simulations to study the mechanical properties of Bracket Set Frames (BSF) in traditional timber structures, proposing a new and effective algorithm to estimate the nonlinear stiffness and horizontal displacement of the frame. Yu et al. (2022) used a nonlinear dynamic analysis to study the energy transfer and dissipation mechanisms in timber frames under lateral seismic activity. Zhang et al. (2023) investigated the seismic performance of traditional Chinese palace-style timber frames based on Discrete Element Modeling (EDEM). The results indicated that the inter-story displacement of column-beam timber frame is the largest, the roof is less, and the Dougong is the least. During minor earthquakes, the structure is most likely to suffer moderate damage. During moderate earthquakes, the structure is prone to severe damage, and during major earthquakes, the structures are likely to collapse.

In actual ancient buildings, timber frames are usually infilled with masonry walls, timber windows, timber doors, and other enclosing structures to form a complete architectural system. Therefore, the study on timber frames with infill walls is important for the comprehensive understanding of the seismic performance of ancient timber buildings. Some scholars studied the impact of infill walls on the mechanical performance, seismic resistance, and stability of timber frames based experimental studies and numerical simulations. Some studies show that the infill walls significantly enhance the load-bearing capacity and seismic performance of timber frames (Xue et al. 2020; Tu 2021). Crayssac et al. (2018) studied the lateral performance of traditional mortise and tenon connected timber frames with and without wooden board infill. The results show that the timber frames exhibit good nonlinear ductility, and the frames with wooden board infill demonstrate higher load-bearing capacity, tangential stiffness, and energy dissipation capability compared with the timber frames without infill structures. Vieux-Champagne et al. (2017) investigated the impact of masonry infill walls on the seismic performance of timber structures and proposed a multi-scale testing scheme. By comparing the test results with those of other similar structures, it is confirmed that the masonry-infilled timber structures exhibit good seismic performance.

To summarize, although considerable progress has been made in recent years by numerous scholars both domestically and internationally in studying the seismic performance of ancient timber structures, research on timber structures with attached doors, windows, and brick walls is less prevalent. Furthermore, the Kanchuang frame is a unique component with national characteristics. However, this part is prone to damage under minor seismic impacts according to the earthquake disaster data (Yuan *et al.* 2022). It is proposed that Kanchuang frame architecture that contains masonry infill walls is inherently vulnerable to brittle cracking of the masonry during seismic effects due to an incompatibility in the much greater ability of the frame to flex without failure compared to the wall material. Based on previous research results, this study takes the Kanchuang frame, which is widely used in Qing-style ancient timber architecture, as the research object. Low-cycle reciprocating load tests were conducted on the Kanchuang frame, and

its seismic performance was studied. A finite element model of the Kanchuang frame was built. Simulation results were compared with test results. Furthermore, the influence of timber friction coefficient, elastic modulus, compressive strength, and vertical loads on the seismic performance of the Kanchuang frame were studied based on the finite element model. Results of this research can provide references for the structural analysis and scientific preservation of ancient timber buildings.

### **EXPERIMENTAL**

# Specimen Design and Fabrication

Based on the prototype of a Kanchuang frame Qing-style ancient timber architecture, a Kanchuang frame model with a scale ratio of 1:2 was fabricated based on "Qing ministry of works: Examples of engineering practices" (Liang 2016) and the "Knowledge manual of Chinese ancient architecture" (Tian 2013). The Kanchuang frame model consists of Fang, columns, Shangkan, window sashes, Fengkan, Taban, Baokuang and masonry wall (Fig. 2). The masonry wall is constructed from Xiaotingni bricks. The components and dimensions of Kanchuang frame are shown in Figs. 3 through 5. *Pinus sylvestris* var. *mongolica*, a commonly used tree species in constructing and renovating ancient timber buildings, was selected to fabricate the model. Moisture content and air-dry density of the wood were 10.09% and 0.396 g/m³, respectively.

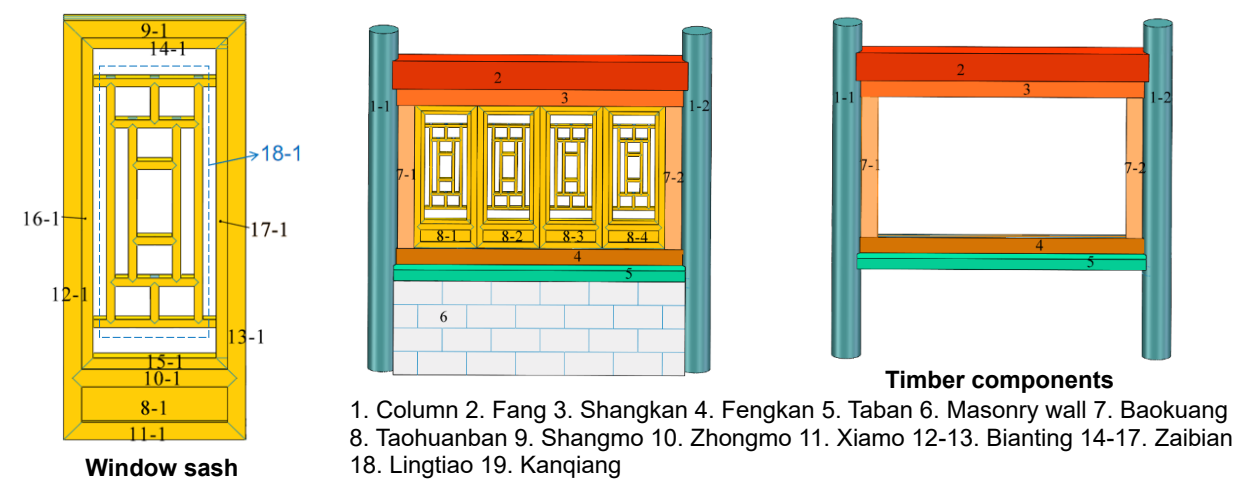
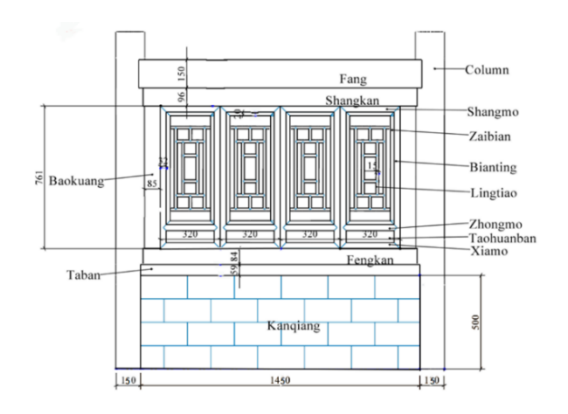
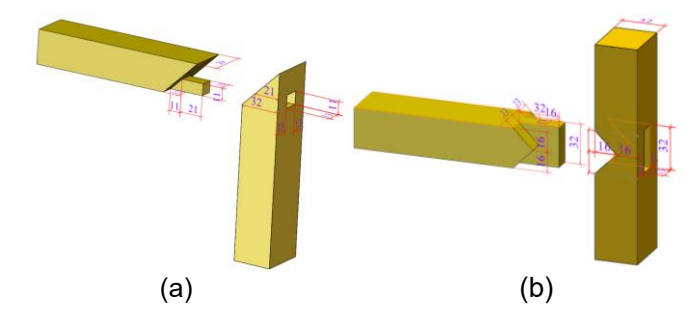


Fig. 2. Components of Kanchuang frame





**Fig. 4.** Dimensions of the mortise and tenon joints (mm): (a) Mortise of the Bianting and tenon of the Shangmo/Xiamo; (b) Mortise of the Bianting and tenon of the Zhongmo

Fig. 3. Dimensions of the test model (mm)

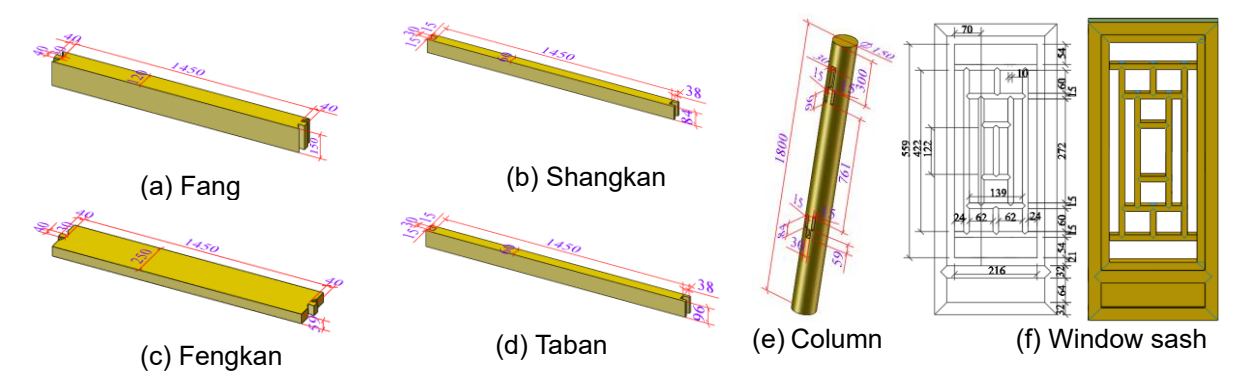


Fig. 5. Dimensions of the specimen (mm)

Mechanical properties of the wood are presented in Table 1. Xiaotingni bricks were selected to build the masonry wall. Xiaotingni bricks are commonly used in Chinese ancient buildings. Traditional lime was used as the masonry mortar. The mechanical properties of the brick masonry were measured according to relevant experimental standards (GB/T 50129 2011; GB/T 2542 2012), and the details are shown in Table 2.

**Table 1.** Mechanical Properties of the Wood

E <sub>L</sub> (MPa)	E <sub>R</sub> (MPa)	E⊤(MPa)	<b>V</b> LR	$oldsymbol{ u}_{LT}$	<b>V</b> RT
8907	1620	771	0.432	0.031	0.749
f <sub>c,L</sub> (MPa)	f <sub>c,R</sub> (MPa)	f <sub>c,⊤</sub> (MPa)	G <sub>LR</sub> (MPa)	G <sub>L⊤</sub> (MPa)	G <sub>RT</sub> (MPa)
46.213	5.493	3.387	468	699	542

Notes: *E*, *v*, *G*, and *f* respectively represent the modulus of elasticity, Poisson's ratio, shear modulus, and strength of the timber. The subscripts L, R, and T refer to the longitudinal, radial, and tangential directions of the wood grain, respectively, while c denotes the compressive state of the timber

**Table 2.** Material Parameters of Masonry

f <sub>c,i</sub> (MPa)	f <sub>v,i</sub> (MPa)	E <sub>c,i</sub> (MPa)	V
3.425	0.041	1259	0.183

Notes:  $f_{c,l}$ ,  $f_{v,l}$ ,  $E_{c,i}$ , and v, respectively, represent the compressive strength, shear strength, modulus of elasticity, and Poisson's ratio of masonry

# **Loading Program**

The roof load of ancient timber structures is transferred sequentially from the rafters to the purlins, from the purlins to the beams, and from the beams to the columns. Based on related literature (Liu 2001a,b; Chen et al. 2016) and similarity theory (Zhou and Lv 2016), the vertical load applied to the top of the column is 12 kN, and the scale factor is 1:4. Steel caps were placed on the top of the columns, and a load distribution beam was placed on the steel caps. To maintain a stable roof load during structural deformation, weight blocks were incorporated at both ends of the distribution beam to simulate the roof loads. This method can make the roof load of the model more closely approximate the actual load. Therefore, a total vertical load of 12 kN was applied to the top of the column *via* the weight blocks hung on both ends of the distribution beam. Research shows (Wang et al. 2018; Zhang et al. 2022) that most columns of Chinese ancient buildings are placed on the foundation stones directly without any other constraints. Under repeated loading, the cyclical lifting and repositioning of the column foot cause the column to sway. This unique structural form can enhance to the seismic energy dissipation capacity of the structure. Based on these characteristics and references (Xie et al. 2020, 2022), the connection at the base of the column was simplified to a hinge in the test model. The timber frame is connected to the steel beam using a steel hinge support, and the inner diameter of the support sleeve matching the diameter of the column. The test loading setup is illustrated in Fig. 6.

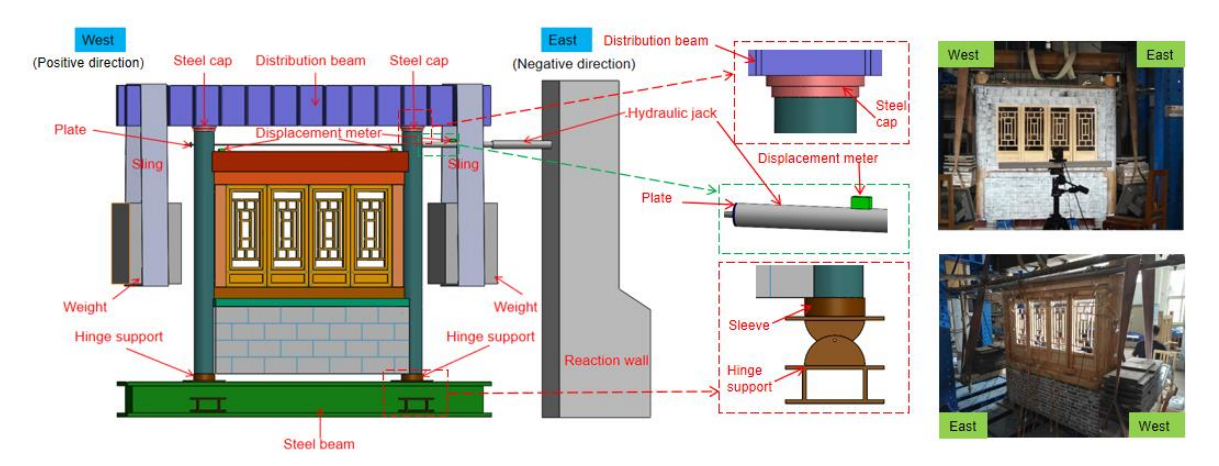


Fig. 6. Test loading setup

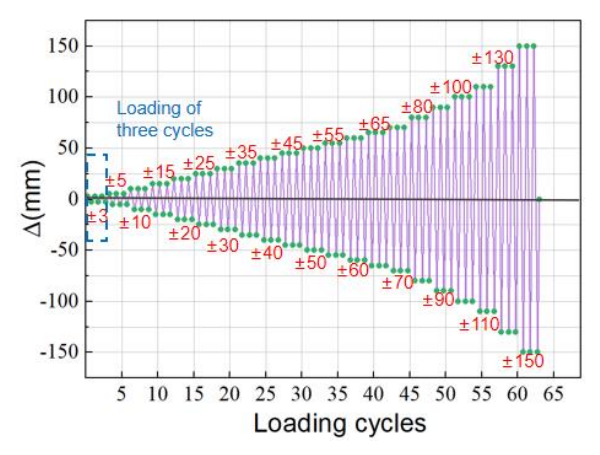
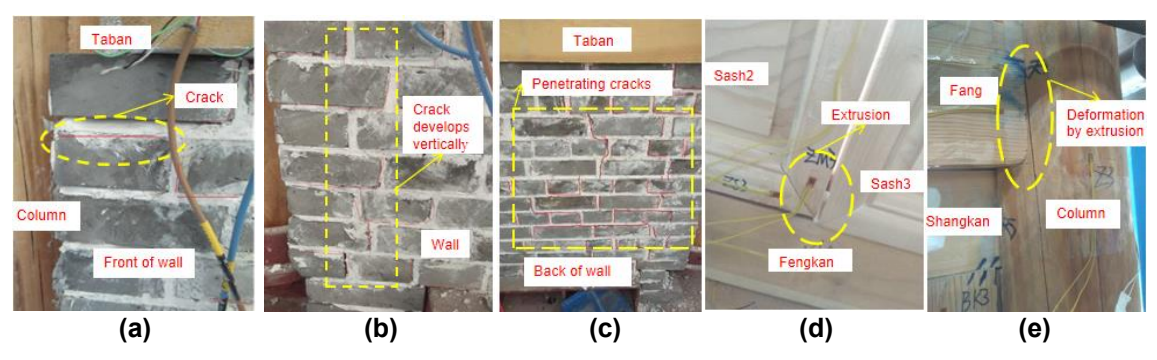


Fig. 7. Loading scheme

The horizontal loads were applied by a jack. The data were collected by displacement, a press sensor, and a computer. There were 21 levels of loading displacements, and the maximum loading displacement was 150 mm. The initial loading displacement was  $\pm$  3 mm. When the loading displacement levels were increased from 5 to 70 mm, the increment in displacement was set at 5 mm. When the displacement levels increased from 70 to 110 mm, the increment for each level was 10 mm. When the loading level exceeded 110 mm, the increment for each control displacement level was 20 mm. Each level of control displacement was repeated three times. Referring to the "Specification for seismic test of buildings" (JGJ/T 101 2015), the loading speed was set at 0.5 mm/s. The loading scheme is shown in Fig. 7.

# **Experimental Phenomena**

During the initial loading displacements levels, when the displacement was between 3 and 5 mm, there was no visible damage observed in the Kanchuang frame. When the loading displacement level reached 20 mm, the timber components made squeaking sounds, and small cracks appeared along the mortar layer at the edges of the top layer of bricks on both sides of the Kangiang. Details are shown in Fig. 8a. When the loading displacement level reached 25 mm, the Kanchuang frame continued to make squeaking sounds. The cracks on the masonry wall developed vertically along the edges on both sides of the wall, the cracks at the bottom of the wall developed upwards, and the cracks at the top extending downwards. Details are shown in Fig. 8b. The cracks on both edges of the wall continued to develop, and the width of cracks gradually increased. When the loading displacement level reached 35 mm, penetrating cracks formed at the edges of the wall, as shown in Fig. 8c. On the Kanchuang frame no visible damages were observed when the loading displacement level was below 40 mm. When the loading displacement reached 50 mm, the cracks in the wall continued to develop, and the window sashes were compressed increasingly tighter and the tenon was slightly pulled out. Details are shown in Fig. 8d. At this point, the timber frame continuously made squeaking sounds due to the compression of the wood. When the loading displacement reached 65 mm, the development of cracks in the wall intensified, and the tenon being pulled out of the mortise of the window sashes continuously increased. The repeated loading made compression between the Fang and the columns increasingly harder and caused plastic deformation at the ends of the Fang. It is shown in Fig. 8e.



**Fig. 8.** Failure modes of specimens: (a) crack on the left side of masonry wall (displacements 20 mm); (b) crack on the masonry wall (displacements 25 mm); (c) through cracks on the right side of the masonry wall (displacements 35 mm); (d) window sash compression (displacements 50 mm); (e) compression deformation of Fang (displacements 65 mm)



**Fig. 9.** Damages of Kanchuang (displacements 150 mm): (a) tenon of Shangmo pulled out of the mortise; (b) compression of wood; (c) compression of Fang; (d) Lingtiao split; (e) Xiamo pulled out of mortise; (f) Crack of Zaibian; (g) tenon of Xiamo pulled out of the mortise; (h) left side of the wall collapsed; (i) right side of the wall collapsed

At the end of the loading scheme, loading displacement level was 150 mm, the wall collapsed, and the Zaibian and Lingtiao of the wooden window was cracked. The tenon of the Zaibian pulled out of the mortise, and the maximum width of the gap was 3 mm. The final failure mode of the specimen structure is shown in Fig. 9.

### **TEST RESULTS AND ANALYSIS**

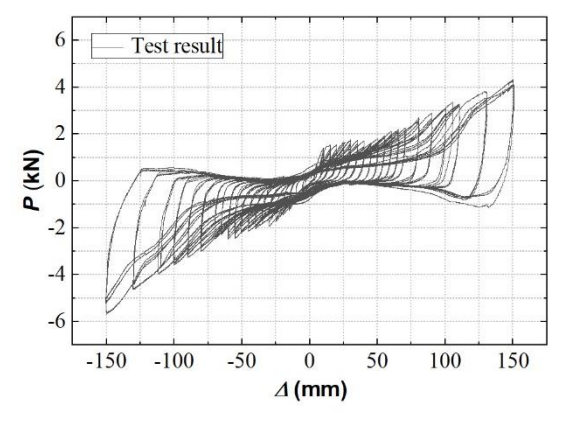
# **Load-displacement Hysteretic Curve**

The load-displacement hysteresis curve of the Kanchuang frame is shown in Fig. 10. Figure 10 shows that the load-displacement hysteresis curve of the Kanchuang frame was Z-shaped, which indicates a 'pinching effect'. The increasing loading displacements and loading cycles exacerbate the 'pinching effect'. This is due to the gaps between the components of the Kanchuang frame. Slip occurred between the components when the loading displacement increased. At the initial loading process, sliding occurred among the components. However, as the loading displacement increased, the components compressed tighter and tighter against each other and the loading forces also increased. With the increasing of loading cycles, the damages and plastic deformations of the Kanchuang timber components and walls accumulated and increased, which made the gaps between the components of the Kanchuang frame wider and wider. That is why the 'pinching effect' was exacerbated. As the loading displacement increased, the middle section of the curves became flatter. When the loading levels were less than 35 mm, the flat feature of the curves was not obvious; When the loading levels were between 35 and 65 mm, the flat feature of the curves gradually became obvious. Once the loading levels exceeded 65 mm (after the wall collapses), all the loads were borne by the wooden components. The intensified plastic deformation of the mortise-tenon joints led to a more pronounced flat segment in the curve. This is mainly because, with the increase of loading displacement, the plastic deformation of wooden components increased, which made the gaps between the mortise and tenon

joints wider and wider. The sliding effect between components was becoming increasingly obvious.

# **Load-displacement Skeleton Curve**

The peak value points of each cycle of load-displacement hysteresis curve were connected to form the load-displacement skeleton curve. The load-displacement skeleton curves of the Kanchuang frame are shown in Fig. 11. Figure 11 shows that the loaddisplacement skeleton curve of the Kanchuang frame can be divided into three stages. Initially, before the loading displacement reached 35 mm, no penetrating cracks appeared in the wall, and the skeleton curves were close to straight lines. This phase is defined as the elastic stage. Subsequently, when the loading displacement level was between 35 mm and 65 mm, the slope of the skeleton curve decreased. At this stage, wall cracks were fully developed and penetrating cracks were formed, and the mechanical performance of the structure began to degrade. This phase is defined as the elastic-plastic stage. Finally, when the loading displacement exceeded 65 mm, the wall began to fall and collapse. The gap between the wall and column became increasingly wider and gradually separated. When the loading displacement level exceeded 60 mm, the wall could not bear the load. Therefore, most of the load is borne by the timber frame, and the skeleton curve of the Kanchuang frame primarily exhibited linear growth. This phase is defined as a new elasticplastic stage. It can be seen that the development of cracks in the masonry wall and the deterioration of the wall's mechanical properties had a negative influence on the mechanical performance of the Kanchuang frame. In the experiment, each level of loading displacement was cycled three times. It was observed that the peak load of the second and third cycles was lower than that of the first. This indicates that cumulative cyclic loading led to the degradation of structural mechanical properties.



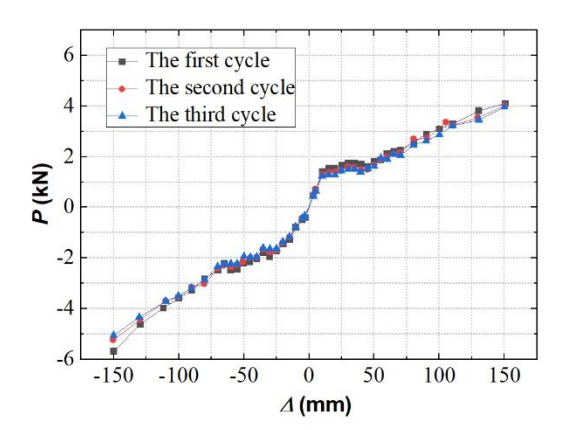


Fig. 10. Load-displacement hysteresis curves

Fig. 11. Load-displacement skeleton curves

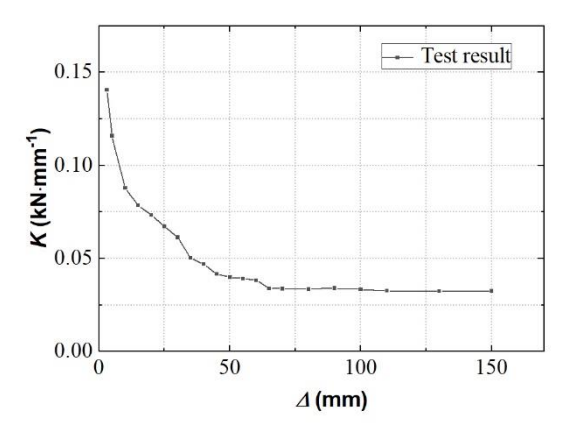
# **Stiffness Degradation**

As the loading displacement increases and cycles increase, the stiffness of the structure decreases. Typically, the secant stiffness (K) is used to represent the stiffness of structure or component under cyclic loading. K can be calculated by Eq. 1,

$$K_i = \frac{\left| +F_i \right| + \left| -F_i \right|}{\left| +\Delta_i \right| + \left| -\Delta_i \right|} \tag{1}$$

where  $F_i$  is the peak load of 1st loading cycle, and  $\Delta_i$  is the corresponding loading displacement. The stiffness degradation curve of the Kanchuang frame shown in Fig. 12.

Figure 12 shows the stiffness gradually decreased with the increase of loading displacement. The curve eventually approached to a horizonal line. Before the loading displacement reached 35 mm, the degradation of stiffness was rapid. After that, the stiffness degraded slowly. And the stiffness of the structure did not change any more when the loading level exceeded 65 mm.



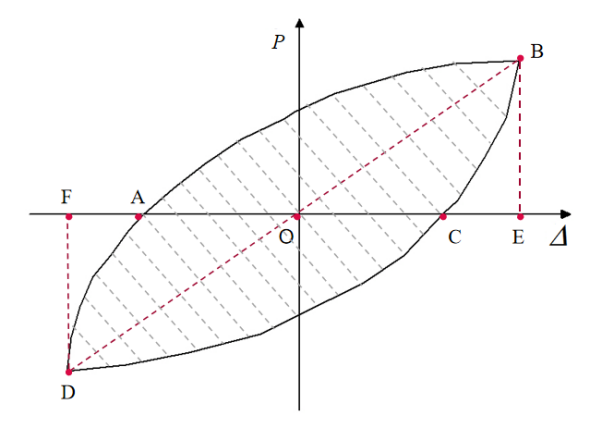


Fig. 12. Stiffness degradation curve

Fig. 13. Equivalent viscous damping coefficient

# **Energy Dissipation Performance**

Energy dissipation capacity refers to the ability of a structure to absorb and dissipate the energy during an earthquake. Commonly, the area of the hysteresis loop or the energy dissipation coefficient is used to measure the structure's energy dissipation capacity. In this part, the equivalent viscous damping coefficient ( $h_e$ ) is used to measure the energy dissipation capacity of the test model. Generally, the larger the energy dissipation coefficient, the stronger the energy dissipation capacity of the structure. The calculation method of the energy dissipation coefficient ( $h_e$ ) is shown in Fig. 13 and Eq. 2.

The formula for calculating the equivalent viscous damping coefficient is as follows,

$$h_{\rm e} = \frac{1}{2\pi} \times \frac{S_{(ABC + CDA)}}{S_{(\Delta OBE + \Delta ODF)}} \tag{2}$$

where S(ABC+CDA) is the area of the hysteresis loop shaded in Fig. 13, and  $S(\Delta OBE+\Delta ODF)$  is the sum of the areas of triangles OBE and ODF. The energy dissipation coefficient of the Kanchuang frame is shown in Fig. 14.

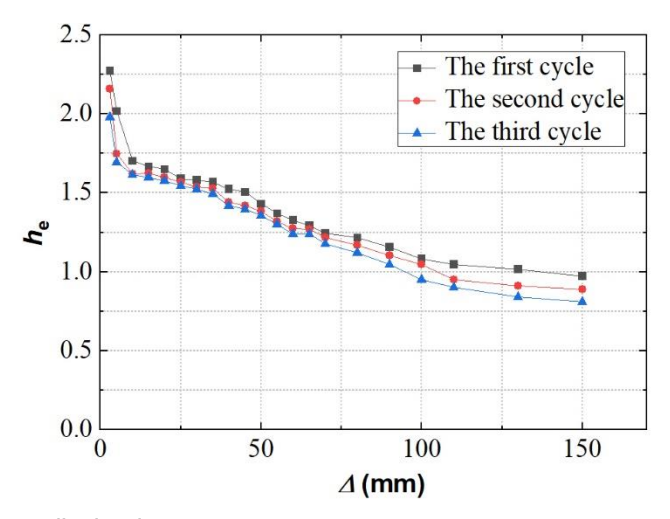


Fig. 14. Energy dissipation curves

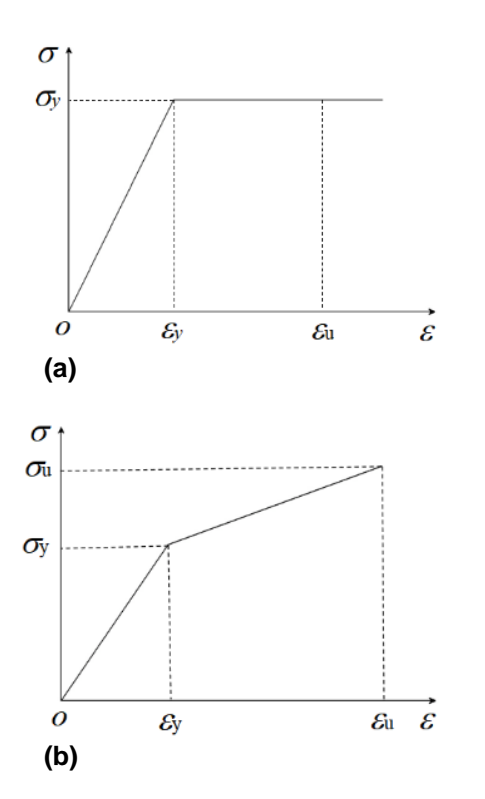


Fig. 15. Constitutive relationship of wood: (a) Parallel to grain; (b) Perpendicular to grain

Figure 14 shows that the energy dissipation capacity of the Kanchuang frame gradually decreased while the loading displacement increased. At the same loading level, the energy dissipation capacity decreased while the loading cycles increased. This indicates that repeated loading process caused mostly by plastic deformation in the timber frame and damage in the masonry wall, which reduced the energy dissipation capacity of the structure. Before the loading displacement reached 35 mm, the energy dissipation capacity of the specimen decreased rapidly. After that, the decrease rate slowed down. This indicates that the development of the cracks in the walls had a noticeable impact on the energy dissipation capacity of the structure.

### FINITE ELEMENT SIMULATION

### **Establishment of Finite Element Model**

A three-dimensional finite element model was established to simulate seismic performance of the Kanchuang frame under horizonal cyclic loads. The material property is one of the main factors that influence the accuracy of the finite element simulation results. Mechanical properties of timber are simplified as orthotropic materials. The ideal elasticplastic model was used to simulate parallel-to-grain compression property of wood, and the bilinear strengthening model was used to simulate perpendicular-to-grain radial compression property of wood (Xue et al. 2019). Details are shown in Fig. 15. During the elastic phase, nine independent engineering constants are used to define the stress-strain relationship of the orthotropic material. These constants include elastic moduli (E), Poisson's ratios (v), shear moduli (G) of the wood along parallel-to-grain directions (L), perpendicular-to-grain radial directions (R), and perpendicular-to-grain tangential directions (T). In the plastic phase, the compressive strength parallel-to-grain is set as the reference yield strength, and the potential function is used to define the initial yield ratios in various directions of the wood to simulate the mechanical properties of the wood (Zhu 2015). Considering the complexity of finite element analysis and calculations, the wall is set as a masonry wall with the mechanical prosperity considered in the finite element model. According to the reference (Tong 2019), compared with other components, the Lingtiao of the window slash has little influence on the whole frame. Therefore, the authors also simplified Lingtiao in the finite element model. The dimensions and material parameters of the finite element model are set the same as the test model.

Eight-node hexahedral linear reduced-integration solid elements (C3D8R) are used to build the finite element model. Surface-to-surface contact is used to simulate the contact between components, and different friction coefficients were set. "Hard contact" is used to define the normal contact between timbers, and Coulomb friction is used to define the tangential forces between the contact surfaces. Research (Yeo et al. 2016) indicates that the friction force between the contact surfaces of mortise and tenon joints plays a significant role in structural vibration reduction and energy dissipation. Mortise-tenon joints are capable of bearing loads as well as allowing rotation, exhibiting semi-rigid properties. Under earthquake excitation and low-cycle reciprocating loading, mortisetenon joints primarily dissipate energy and mitigate vibrations through dynamic friction. Therefore, when conducting finite element simulation of the structure, dynamic friction coefficients are typically adopted in the model. According to relevant research (Ma and Zhao 2012), the friction coefficient between timbers usually ranges from 0.1 to 0.65. Some studies show that the friction coefficient between timbers is approximately 0.5 (Xie et al. 2018). Therefore, the friction coefficient is set as 0.5 in the finite element model. Compared with masonry wall, mortise and tenon joints are basically in elastic-plastic deformation stage, especially in the contact surfaces area. Other parts of components that are farther away from the joints, such as middle part of Fangs and columns, are generally in elastic deformation state. Therefore, smaller mesh sizes are used at the connection joints and larger mesh sizes are used at other parts to get more realistic simulation results and improve the computational efficiency at the same time. The tenon's surface is set as the master surface, and the mortise's surface is set as the slave surface. To prevent the master surface from penetrating the slave surface, the element mesh sizes of the mortise and tenon contact surfaces are 10 and 20 mm, respectively. The mesh sizes of elements further from the contact areas are 20 and 30 mm, respectively.

Reference points are defined at 100 mm vertical away from the bottom and top surfaces of the model. All the reference points are coupled with the corresponding surfaces. Details are shown in Fig. 16. The bottom of the columns is connected with the base by a hinged support, which constrains horizontal displacement of the model. A vertical load of 6 kN is applied on the top of each column to simulate the roof load. The bottom surface of the masonry wall is fixed on the base, translational, and rotational movements in all three directions are constrained. A reference point is set at 100 mm from the right column and is coupled with the lateral surfaces of the two columns above the beam. At this reference point, cyclic reciprocating horizonal load is applied. The finite element model and boundary conditions are shown in Fig. 16.

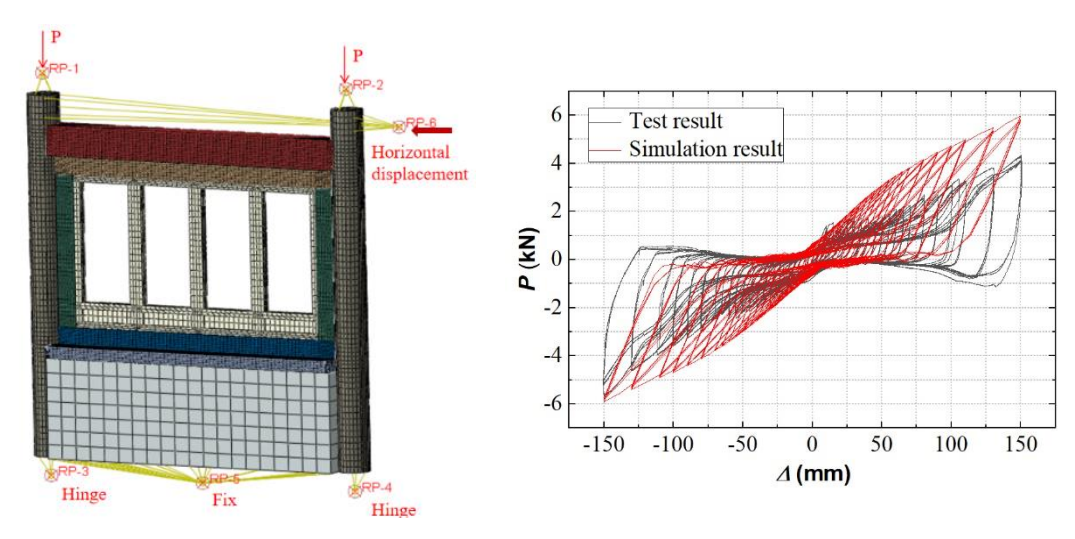


Fig. 16. Meshing and boundary constraints of finite element model

Fig. 17. Hysteresis curves

# **Comparison and Verification of Finite Element Model**

Load-displacement hysteretic curve

A comparison of simulated and test load-displacement hysteresis curves is shown in Fig. 17. The test results curves and the simulation curves are Z-shaped, the pinching effect is obvious, and the changing trends of both curves are the same. At the initial loading stage, the increasing rate of the force shown in the hysteresis test results curves is lower than that of finite element calculations. This is mainly because there are initial gaps between components of the test model, and slippage occurs between the surfaces of the components during the loading process. However, the gaps are not considered in the FEM for the complex contact conditions. Consequently, the amount of slippage between the components in the test model is more than that in the finite element model. As the loading displacement and the loading cycles increase, the structural forces continue to grow, and the difference of forces between the test results and the simulation results steadily decreases. The unloading stiffness of the test results is greater than the simulation results. This mainly because homogeneous ideal materials are used in finite element simulation without considering the natural initial flaws of the wood. The studies of An et al. (2024) and Zhang et al. (2023) also show the same results. Figure 17 shows the hysteresis curves of the finite element simulation results are symmetrical, while the test results are slightly asymmetrical. This is mainly due to three reasons. First, the wood of test specimens has unavoidable natural defects, while the material in the finite element model is ideal. Second, the test structures are not perfectly symmetrical. There are errors during the manufacturing and installation process. However, in the simulation process the loading is absolutely symmetrical. Overall, the general trend and changing rules of both results are the same.

# Load-displacement skeleton curve

The comparison between the test results and the simulation results of the skeleton curves is shown in Fig. 18. Figure 18 shows that the skeleton curves of the test results are a bit asymmetry in the positive and negative loading directions. A skeleton curve is the line connecting the peak values of the hysteretic curve under various displacement loading levels. At the initial loading stage, the initial stiffness values of the test and simulation results are basically the same. In both positive and negative loading directions, the test values and the simulated values are basically the same before the loading displacement reaches 30 mm. At this stage, little damage had occurred in the masonry wall, and the slopes of both curves are large. It indicates the stiffness of the structure is large at this stage. In the later subsequent loading process, both the test and simulation load values increase with the increase of loading displacement. However, the slope of the curves is decreased with the increase of the loading displacement. The simulation results are slightly bigger than the test results. This is mainly because the material parameters used in the FEM are uniform and ideal without natural initial defects. Further, the dimension errors and gaps between components are not considered in the simulation model. When the loading displacements are between 30 to 65 mm, the test results curves show a decreasing trend, while the simulation curve does not. This is mainly because under the cyclic loading process, the damages of test masonry wall accumulated, and the wall cracks and gradually collapses. Moreover, the gaps between the masonry wall and columns are increasingly wider. The wall is no longer involved in bearing loads. As the loading displacement increases, penetrating cracks developed in the wall, leading to rapid degradation of mechanical properties. In the simulation, although the wall reaches the plastic deformation stage and the plastic deformation is formed, the meshes do not collapse or fall apart, which still could bear compressive forces. When the positive loading displacement reaches 150 mm, the error between the simulated values and the test values is the largest. The error is about 32.3%. Although there are errors between test results and finite element simulation results, the changing trend of the curves is the same.

### Stiffness degradation

The comparison between the stiffness degradation curves of the test results and the finite element simulation results is shown in Fig. 19. Both the test and simulated stiffness values decrease with the increase of loading displacement. The stiffness degradation is mainly because the irreversible plastic deformation occurs and accumulate in the structure while the loading displacement and cycles increase. Before the loading displacement reaches 35 mm, the stiffness values of both the test and simulation results decrease rapidly. When the loading displacement exceeds 35 mm, the decrease rate of both curves is less than that when the loading displacement is below 35 mm. The finite element simulation results are slightly greater than the test results. When the loading displacement reaches 65 mm, the stiffness values of the test results and the simulation results are quite different. The error was about 39.4%. This is because in the idealized FEM there are no original gaps

between components and natural imperfections of the material. Because the boundaries and contact conditions of the finite model are complex, if all conditions are considered, the calculation will take time and the results likely will not converge.

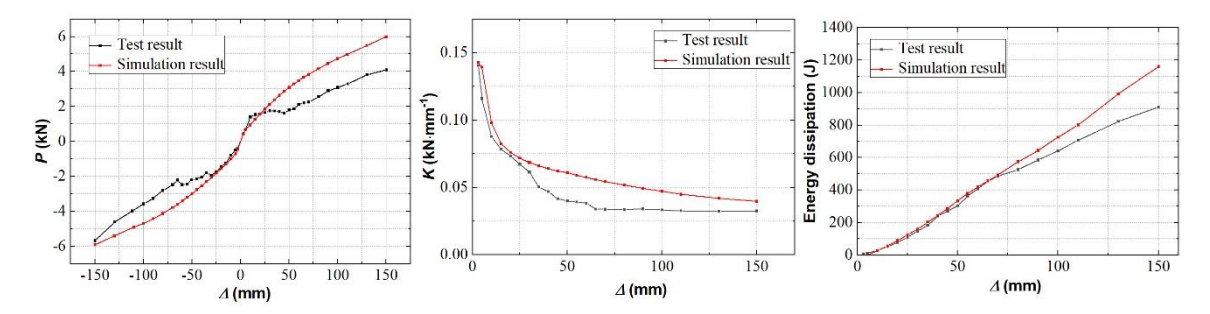


Fig. 18. Skeleton curves

Fig. 19. Stiffness degradation curves

Fig. 20. Energy dissipation curves

Energy dissipation performance

The area of the hysteresis curve can be used to evaluate the energy dissipation capacity of structures. The following sections of this article use the cumulative energy dissipation method to assess the energy dissipation capacity of Kanchuang frame. The cumulative energy dissipation capacity of the model is evaluated by the sum area of the hysteresis curve after three cycling loading displacements at every loading level. The cumulative energy dissipation curves of both the test and simulation results are shown in Fig. 20. The curves of both results are increased with the increase of loading displacement as a whole. The simulation results were quite close to the experimental results. When the loading displacement was less than 10 mm, both the test and simulation values were small. At this phase, the structure was in elastic deformation stage and no damage occurred. When the loading displacement ranged from 10 to 80 mm, the results of the finite element calculations were close to the test results, but slightly bigger than the test values. At this phase, the masonry wall began to crack, and the cracks became increasingly wider while the loading displacement increased. Although the wall damage was increasing, the wall was not collapsed and could bear the compression loads. However, when the loading displacement exceeded 80 mm, the differences between the finite element calculations and the test results increased. This is due to the damage and plastic deformation accumulation of the wall, which caused mortar and fragments of bricks to fall off from the wall. This made the gaps between the wall and column increasingly wider in the test. In the FEM, the material of the wall is in an ideal state with tighter component contacts with the column, which made the dissipated energy in the simulation bigger than that of test.

# Stress Analysis

The stress distribution of the model is shown in Figs. 21 and 22. From the overall contour map of the Kanchuang frame, it can be observed that the maximum compressive stress is 22.33 MPa. Under repeated loading, frictional sliding occurs between the wooden components. The timber components squeeze with each other.

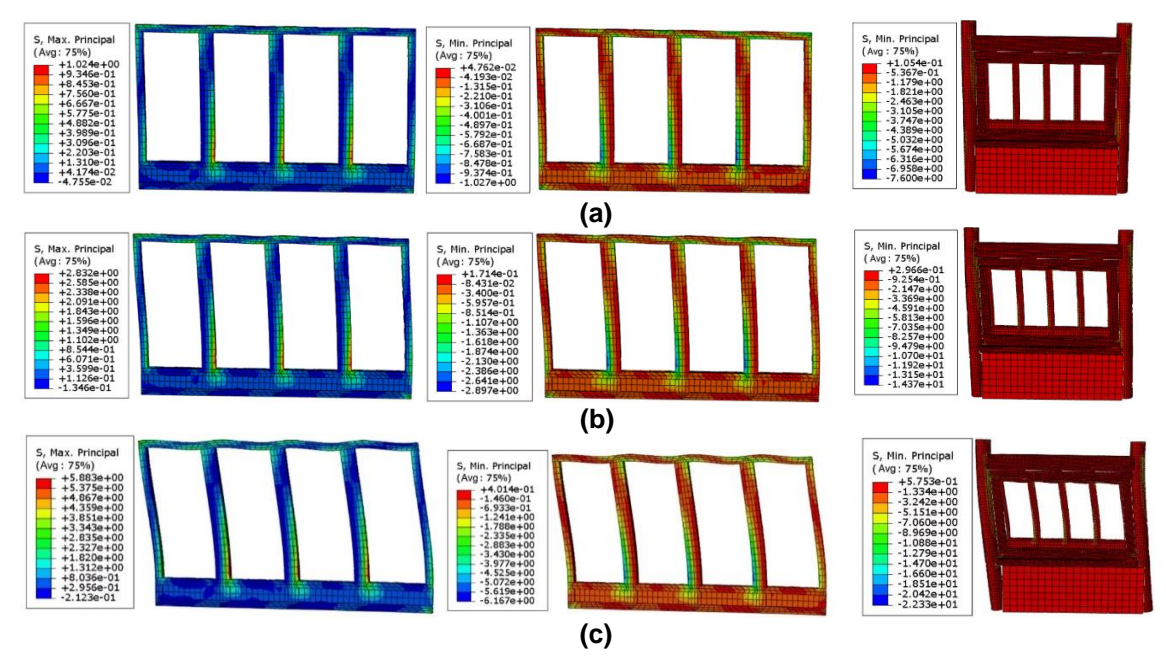


**Fig. 21.** Stress diagram of the sash and at the model at positive loading displacement: (a) 20 mm; (b) 60 mm; (c) 150 mm

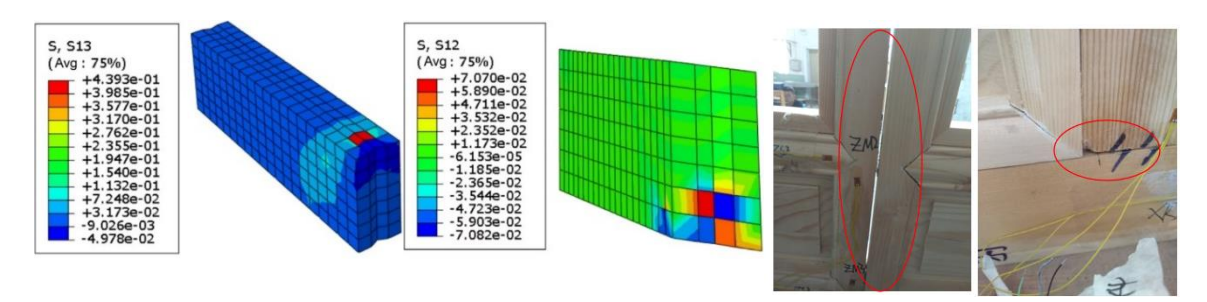


Fig. 22. Stress diagram of the wall at positive maximum loading displacement (150 mm)

**Fig. 23.** Banting compression deformation

Figure 21 shows the Bianting of the windows are compression deformed; this phenomenon is consistent with the experimental phenomena that were observed. The details are shown in Fig. 23. The stress distribution of the windows show that the maximum tensile and compressive stresses are 5.88 and 6.17 MPa, respectively. The maximum compressive strain of the window is located at the intersection of Zhongmo and Zaibian. The maximum compressive strain of the Fang, Shangkan, Fengkan, and Taban is located at the area near the joint that connects with the column. During the loading process, sliding friction occurs between the Taban and the top of the brick wall. Additionally, during the loading process, the wall and column squeeze each other. However, the elastic modulus of the wall and column is different. Therefore, when the loading displacement is large, there are gaps between the column and masonry wall. The stress at the contact surfaces between the brick wall and the Taban and the column is obvious. This is consistent with the deformation and damage characteristics of test phenomenon (Fig. 9).

# **Parameter Analysis**

To further investigate the seismic performance of Kanchuang frame, parameter analysis was conducted based on the finite element model. This analysis studies the effects of the friction coefficient, elastic modulus, compressive strength in parallel-to-grain directions, and vertical load on the seismic performance of the Kanchuang frame.

# Timber friction coefficient

Under horizontal cyclic loads, the Kanchuang frame could dissipate the seismic energy by frictional sliding between components. Studies show that the friction coefficients between the contact surfaces of timber range from 0.1 to 0.65 (He *et al.* 2017). The values of friction coefficient are determined by the tree species and roughness of the contact surfaces. Timber friction coefficients were set as 0.2, 0.3, 0.4, 0.5, and 0.6 in the FEM to investigate their impact on the seismic performance of the Kanchuang frame.

The load-displacement hysteretic curves, skeleton curves, stiffness degradation curves, and cumulative energy dissipation curves of Kanchuang frame with different assumed timber friction coefficients are shown in Fig. 24. Figure 24a shows that as the timber friction coefficient increases, the ultimate forces and the hysteresis loop area of the structure increase. This is because a higher friction coefficient results in rougher contact surfaces between components. The tighter contact and squeeze lead to greater compressive deformation between components, and the bigger forces result in more energy dissipated. When the wood friction coefficients are different, the changing trends of the skeleton curves are basically the same. Details are shown in Fig. 24b. All the curves decrease rapidly at first, then decrease slowly, until they become stable and smooth at last. The forces of the Kanchuang frame increase while friction coefficient increases. When the friction coefficient increases from 0.2 to 0.6, the positive load- forces of the Kanchuang frame increases by 19.46%, 38.1%, 56.85%, and 70.01%. The negative load-bearing capacity increases by 19.14%, 38.16%, 56.01%, and 68.57%. Therefore, the impact of the friction coefficient on the horizonal loads of the Kanchuang frame is greater when the value increases from 0.3 to 0.5. Figure 24c shows as the load displacement increases, the stiffness of Kanchuang frame with different timber friction coefficients decrease. Before the load displacement reaches 20 mm, the rate of stiffness degradation is rapid. When the loading displacements exceed 20 mm, the decline rate of stiffness tends to slow down and gradually keep steady at last. Figure 24c indicates that the stiffness of Kanchuang frame increases with the increase of the timber friction coefficient. With each 0.1 increase in the friction coefficient, the increments of initial stiffness are 32.95%, 2.62%, 1.35%, and 0.77%, respectively. The increments gradually decrease while the loading displacement increase. When the timber friction coefficient ranges from 0.3 to 0.6, its impact on the initial stiffness of the Kanchuang frame is relatively minor. At the same loading displacement level, the energy dissipation capacity of the Kanchuang frame increases with the increase of timber friction coefficient. Details are shown in Fig. 24d. Before the loading displacement reaches 35 mm, the difference in cumulative energy dissipation of Kanchuang frame with different timber friction coefficients is relatively small. However, the difference increased when the loading displacement exceeds 35 mm. When the timber friction coefficient increases from 0.2 to 0.6, the maximum cumulative energy dissipated at each level is 260.27, 333.27, 399.59, 454.66, and 489.92 J, respectively. It is clearly observed that when the timber friction coefficients are between 0.2 and 0.5, the impact of the timber friction coefficient on the energy dissipation capacity of the Kanchuang frame is larger than other friction coefficients.

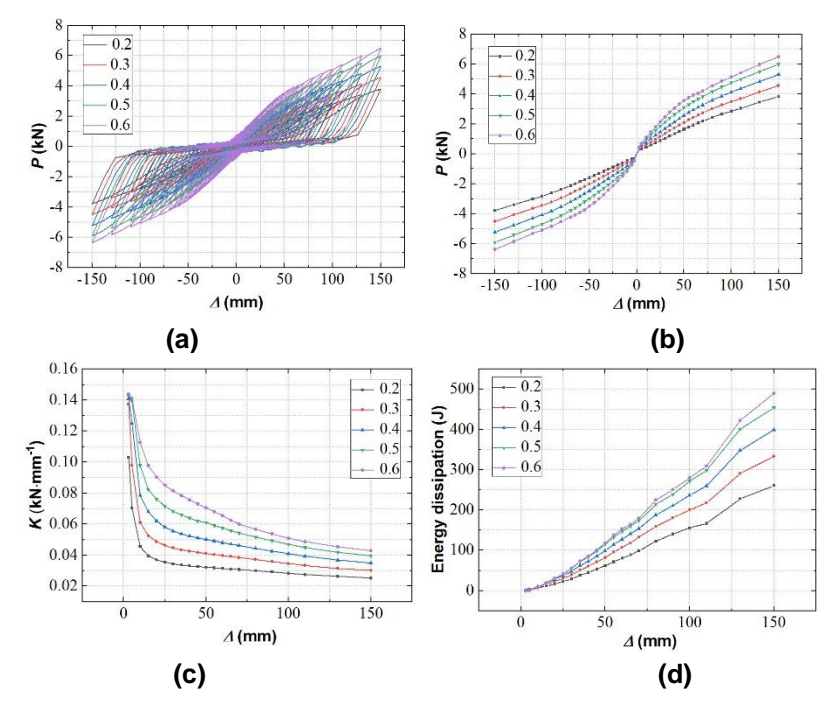


**Fig. 24.** Simulation results of different friction coefficients: (a) Hysteresis curves; (b) Skeleton curves; (c) Stiffness degradation curves; (d) Energy dissipation curves

# **Elasticity Modulus**

To study the impact of the elastic modulus on the seismic performance of Kanchuang frame, while other parameters are the same, the elastic moduli were adjusted in the element model. Ratios of 0.60, 0.80, 1.00, 1.20, and 1.40 times the tested elasticity modulus in perpendicular-to-grain radial directions  $E_R$  and elasticity modulus in parallel-to-grain directions  $E_L$  of the test wood material are set in the FEM to study their effects on the structural performance of the Kanchuang frame.

Elasticity modulus in perpendicular-to-grain radial directions

Figure 25 shows the radial modulus of elasticity in the perpendicular-to-grain direction has minor impact on the seismic performance of the structure. Figure 25b shows the difference between the skeleton curves of the Kanchuang frame with different radial moduli of elasticity in the perpendicular-to-grain direction are small. It is indicated that the modulus has little effect on the stiffness of the frame, which is also reflected in Fig. 25c. When the horizontal displacement exceeds the elastic stage (loading displacement exceeds 35 mm), in the positive loading direction, every 20% increase in the radial modulus of in the perpendicular-to-grain direction leads to 1.59%, 1.02%, 0.91%, and 0.64% increases in the peak loads, respectively.

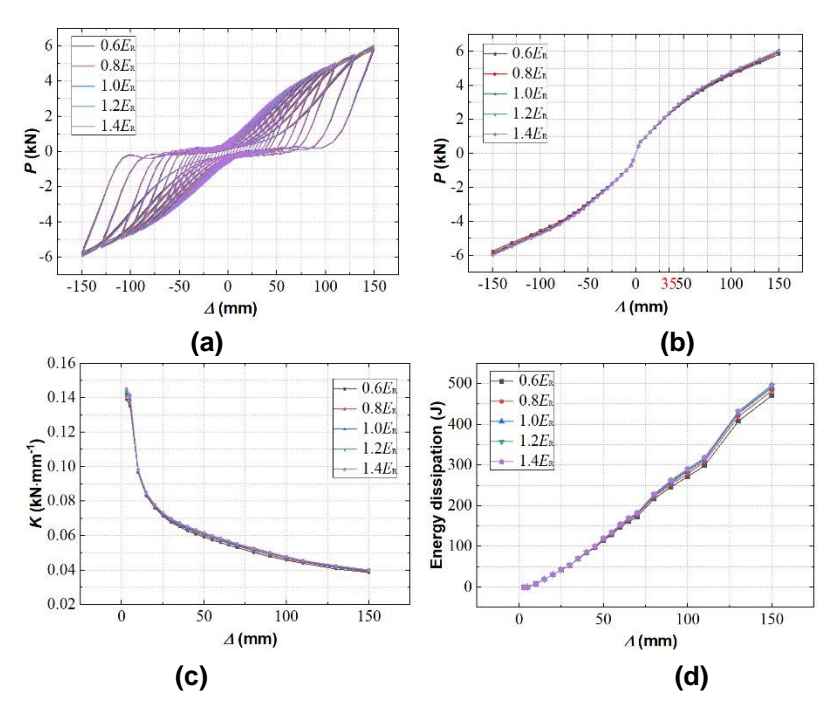


**Fig. 25.** Simulation results of different elasticity modulus in perpendicular-to-grain radial directions: (a) Hysteresis curves; (b) Skeleton curves; (c) Stiffness degradation curves; (d) Energy dissipation curves

In the negative loading direction, every 20% increase in radial modulus of elasticity in the perpendicular-to-grain direction leads to 1.72%, 0.97%, 0.90%, and 0.63% increases in peak loads. This indicates that the radial modulus of elasticity in the perpendicular-to-grain direction has a positive impact on the seismic performance of the structure; however, the impact is small. Figure 25d shows the cumulative energy dissipation capacities of the Kanchuang frame with different radial moduli of elasticity in the perpendicular-to-grain direction. When the loading displacement is above 80 mm, the cumulative energy dissipation values of the frames with different radial moduli of elasticity are basically the same. However, once the loading displacement exceeds 80 mm, the differences begin to show between cumulative energy dissipation values of the frames increase with different radial modulus of elasticity in the perpendicular-to-grain direction. Specifically, as the radial modulus of elasticity increases from  $0.6 E_R$  to  $1.4 E_R$ , the maximum cumulative energy dissipation values increase 2.63%, 4.20%, 5.08%, and 5.61%, respectively.

# Elasticity modulus in parallel-to-grain directions

The hysteresis curves, skeleton curves, stiffness degradation curves, and cumulative energy dissipation curves of Kanchuang frame with different elasticity moduli in parallel-to-grain directions are shown in Fig. 26. It can be observed that with the increases of the parallel-to-grain elasticity modulus, the peak loads, initial stiffness, and energy dissipation capacity of the Kanchuang frame increase. Further, the increases of the peak values and stiffness are larger than that of in perpendicular-to-grain radial directions. At the same loading displacement, the higher the elasticity modulus in the parallel-to-grain direction, the greater the structural stiffness and energy dissipation capacity of the Kanchuang frame.

Compared with the modulus set at  $0.6~E_L$ , when the parallel-to-grain elasticity modulus is set at  $0.8~E_L$ ,  $1.0~E_L$ ,  $1.2~E_L$ , and  $1.4~E_L$ , the ultimate peak loads of the Kanchuang frame increase by 9.74%, 21.16%, 31.78%, and 41.52%, respectively. Additionally, the initial stiffnesses increase by 2.06%, 18.82%, 36.01%, and 51.62%, respectively. Consequently, it is evident that within this range, for every 20% increase in the parallel-to-grain elasticity modulus, there is an average increase of 10.38% in the ultimate peak loads of the Kanchuang frame.

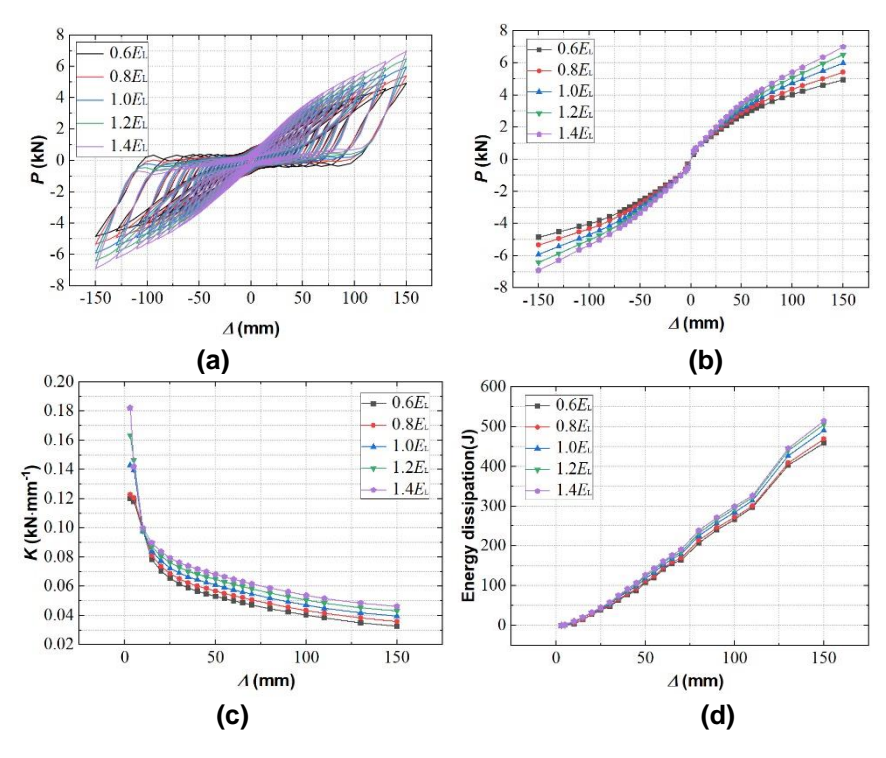


**Fig. 26.** Simulation results of different elasticity modulus in parallel-to-grain directions: (a) Hysteresis curves; (b) Skeleton curves; (c) Stiffness degradation curves; (d) Energy dissipation curves

### Compressive strength in parallel-to-grain directions

Compared with the elasticity modulus in perpendicular-to-grain radial directions the modulus of elasticity in parallel-to-grain directions have greater impact on the seismic performance of the frames. Therefore, to study the effect of compressive strength on the seismic performance of Kanchuang frame, while other parameters are the same, the compressive strength along the parallel-to-grain directions of the wood is adjusted proportionally. Ratios of 0.60, 0.80, 1.00, 1.20, and 1.40 times of the measured compressive strength along the parallel-to-grain directions  $f_{\rm cL}$  are set in finite element simulation to investigate their impact on the seismic performance of the frames.

The load-displacement hysteresis curves of the Kanchuang frame with different parallel-to-grain compressive strengths are shown in Fig. 27a. The figure shows the ultimate peak loads, stiffnesses, and the hysteresis loop area of the frames increase with the increase of the parallel-to-grain compressive strength. When the loading displacement reaches the ultimate displacement, the positive and negative ultimate peak loads of the structure with parallel-to-grain compressive strength of  $0.6\,f_{\rm cL}$  are  $4.64\,{\rm kN}$  and  $4.56\,{\rm kN}$ , respectively. Compared with the simulation results of the structure with the parallel-to-

grain compressive strength of  $0.6\,f_{\rm cL}$ , the positive ultimate peak loads with parallel-to-grain compressive strengths set as  $0.8\,f_{\rm cL}$ ,  $1.0\,f_{\rm cL}$ ,  $1.2\,f_{\rm cL}$ , and  $1.4\,f_{\rm cL}$  increase 15.86%, 11.15%, 9.06%, and 7.18%, respectively. The negative ultimate peak loads increase by 16.20%, 11.48%, 9.05%, and 7.39%, respectively. Details are shown in Fig. 27b, which shows that parallel-to-grain compressive strength has a positive impact on the ultimate peak loads of the structure.

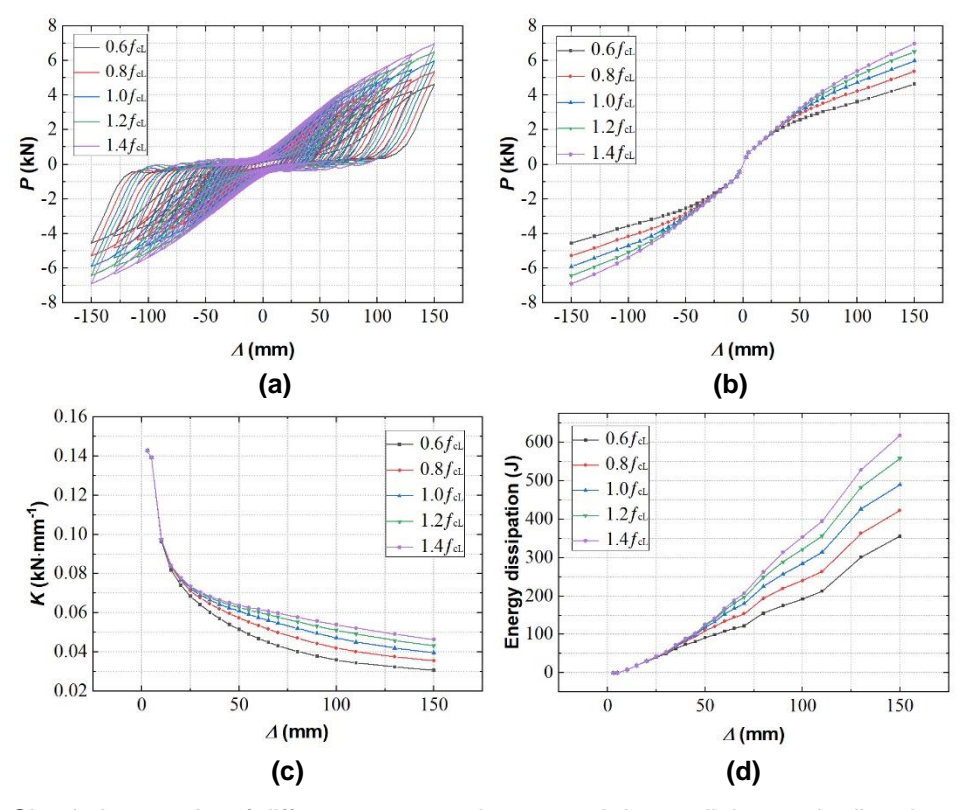


**Fig. 27.** Simulation results of different compressive strength in parallel-to-grain directions: (a) Hysteresis curves; (b) Skeleton curves; (c) Stiffness degradation curves; (d) Energy dissipation curves

It can be clearly observed that parallel-to-grain compressive strength has little impact on the initial stiffness on the structure. All the stiffness values of the structure with different parallel-to-grain compressive strengths decrease as the loading displacement increases. When the loading displacement exceeds 15 mm, at the same loading displacement, the higher the parallel-to-grain compressive strength, the greater the stiffness of the Kanchuang frame. Details are shown in Fig. 27c. Figure 28d shows the increase in parallel-to-grain compressive strength enhances the energy dissipation capacity of the Kanchuang frame. When the parallel-to-grain compressive strength increases from  $0.6 f_{\rm cL}$  to  $1.4 f_{\rm cL}$ , the maximum cumulative energy dissipation values increase by 18.73%, 27.68%, 56.71%, and 73.51%, respectively.

### Vertical load

A distinctive characteristic of ancient architectural timber structures is their artistic large roofs. The grand roof truss system enhances the overall seismic performance of the structure. It also provides excellent constraint to the columns (Jacklin *et al.* 2014). Moreover, the grand roof truss system distributes vertical loads to the beams or columns.

It minimizes the gaps at the mortise and tenon joints and provides sufficient friction. In addition, it strengthens the overall stability of the building (Chen 2016). Ratios of 0.60, 0.80, 1.00, 1.20, and 1.40 times of the vertical loads applied on the test model *N* were set in finite element simulation model to investigate their impact on the seismic performance of the frames.

Figure 28 shows that the vertical loads affect the ultimate peak loads, stiffness, and energy dissipation abilities of the Kanchuang frame. The ultimate peak loads of the structure decrease with the increase of vertical load. Every 20% increase in vertical load, the positive and negative ultimate peak loads decrease by 3.74% and 3.65%, respectively.

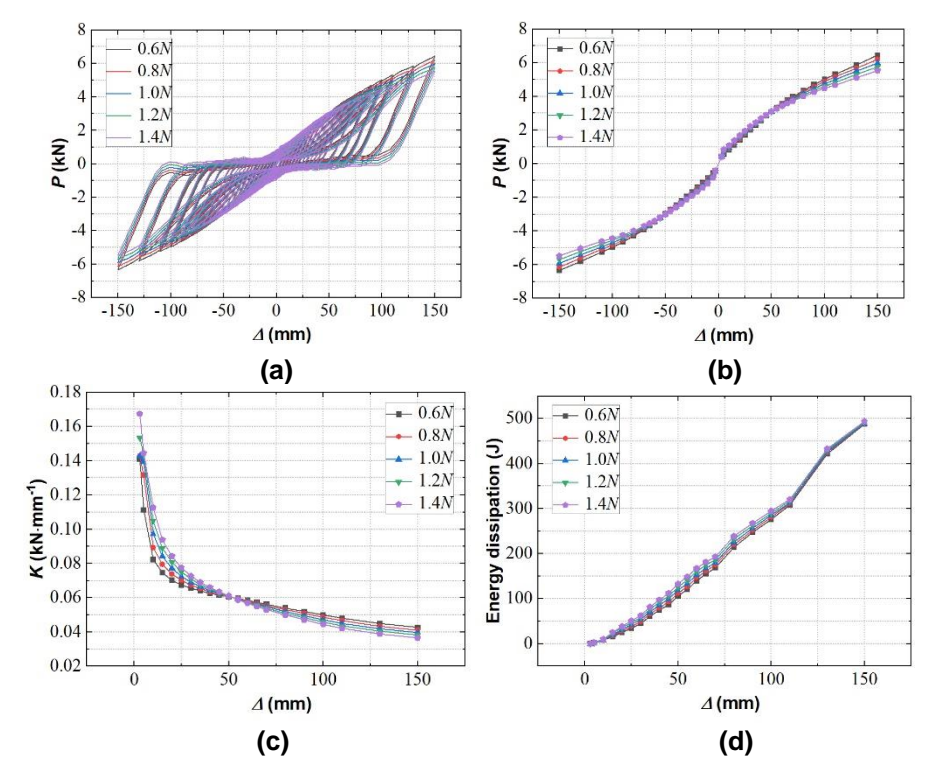


**Fig. 28.** Simulation results of different vertical load: (a) Hysteresis curves; (b) Skeleton curves; (c) Stiffness degradation curves; (d) Energy dissipation curves

Both the initial stiffness of the structure increase with the increase in vertical load. When the vertical load is increased from 0.6 N to 1.4 N, the initial stiffness increases by 0.02%, 1.14%, 7.41%, and 9.15% at different loading levels. The stiffness decreases with the increase of vertical loads when the loading displacement exceeds 65 mm.

Through comparing the cumulative energy dissipation curves with different vertical loads, Fig. 28(d) shows when the vertical loads increase, the structure has to dissipate more energy. The differences are minor before the loading displacement reaches 15 mm. Moreover, when the loading displacement reaches 20 mm, the differences between different curves gradually become prominent When the loading displacement is between 35 mm and 90 mm, the differences of the curves with different vertical loads is more obvious. When the loading displacement exceeds 100 mm, the differences become minor.

### CONCLUSIONS

This paper aimed to investigate the seismic performance of Kanchuang frame timber structures with masonry wall infill based on low-cycle reciprocating load test and finite element analysis. The following conclusions are drawn:

- 1. During the loading process, the wall cracks and fails before the wooden components. The damage to the wooden components is mainly manifested as joint pull-out (of tenons). After they all fail, the timber structure can still sustain loads. This means that in the seismic event, the wall cracks formed during the initial seismic impulse while the wooden components are basically intact or slightly damaged. The structure exhibits vulnerability to damage under minor earthquakes but possesses good anti-collapse performance under major earthquakes.
- 2. The hysteresis curve of the Kanchuang frame shows a Z-shape with a pinching effect, which indicates slip occurred between timber components. As the loading displacement increases, the load-stiffness of the structure decreases and ultimate peak values increase. It shows that the timber structural frame has good load bearing and deformation capacities.
- 3. Both the simulation results and the test results show that after the wall fails the structure can continue to bear the loads. Compared with the masonry wall, the timber part of the Kanchuang frame has higher bearing and deformation capacities. The finite simulation results were basically consistent with the test results despite some errors.
- 4. The ultimate peak loads, stiffness, and energy dissipation capacity of the Kanchuang frame increase with the increase of the timber friction coefficient, the elastic modulus in the parallel-to-grain and perpendicular-to-grain directions, and the compressive strength in the parallel-to-grain direction. However, the influence of perpendicular-to-grain radial elastic modulus of the wood is minor.
- 5. The vertical loads have positive impact on the initial stiffness and energy dissipation capacity of the structure, but have negative effect on the ultimate peak loads and ultimate stiffness of the structure.

To improve the accuracy of finite element analysis, how to introduce defects into the finite element analysis process will be a key issue that we need to work on in the future.

### **ACKNOWLEDGMENTS**

This study was supported by the independent project of the School of Civil Engineering, Shijiazhuang Tiedao University (No. TMXN2301), Basic Research Funds of Shijiazhuang University (No. ZQK202402), National Key R&D Program of China (Grant No. 2019YFC1520803), Beijing Municipal Commission of Education-Municipal Natural Science Joint Foundation: "Research on Seismic Performance Evaluation of Beijing Ancient Timber Buildings Based on Value and damage Characteristics" (No. KZ202010005012), National Natural Science Foundation of China (No. 52278472, 2019YFC1520803), Beijing Municipal Natural Science Foundation (No.8232004), Central guidance for local scientific and technological development funding projects (No. 246Z5410G).

### REFERENCES CITED

- An, R. B., Yuan, J. C., Pan, Y., and Yi, D. H. (2024). "Experimental study on the seismic performance of a full-scale two-story traditional timber frame on sloped land," *Engineering Structures* 300, article ID 117139. DOI: 10.1016/j.engstruct.2023.117139
- An, R. B., You, W. L., Pan, Y., and Liu, S. Y. (2022). "Seismic damage investigation and analysis of cultural heritages in M\_s 6.0 Luxian earthquake," *China Civil Engineering Journal* 55(12), 13-24. (in Chinese). DOI: 10.15951/j.tmgcxb.21111071
- Bai, F. Y., Dong, F., Sui, Y., Xue, J. Y., Wu, C. W., Song, D. J., and Hu, C. M. (2023a). "Experimental study on fracture damage and seismic performance of loose throughtenon joints in ancient timber structures," *Construction and Building Materials* 394, article ID 132228. DOI: 10.1016/j.conbuildmat.2023.132228
- Bai, F. Y., Fan, Z. K., Xue, J. Y., Wu, C. W., Hu, C. M., and Li, J. X. (2023b). "Experimental study on seismic performance and deformation damage of loose dovetail-tenon joints in ancient timber structures," *Structures* 54, 541-555. DOI: 10.1016/j.istruc.2023.05.059
- Ben, S., Wang, H., and Li, A. Q. (2019). "The influence of the damage of mortise-tenon joint on the cyclic performance of the traditional Chinese timber frame," *Applied Sciences* 9(16), article 3429. DOI: 10.3390/app9163429
- Chen, C. C. (2016). *Integral Mechanics Property Analysis and Safety Evaluation of Ancient Timber Structures*, Master's Thesis, Southeast University, Jiangsu, China.
- Chen, J. Y., Shi, X. W., Niu, Q. F., Wei, J. W., Li, T. Y., and Zhao, Y. X. (2016). "Analysis of similar Cai Fen modular system based on the weight of the roof of Song dynasty," *Journal of Civil and Environmental Engineering* 38(05), 27-33. DOI: 10.11835/j.issn.1674-4764 2016.05.004
- Crayssac, E., Song, X. B., Wu, Y. J., and Li, K. (2018). "Lateral performance of mortise-tenon jointed traditional timber frames with wood panel infill," *Engineering Structures* 161, 223-230. DOI: 10.1016/j.engstruct.2018.02.022
- GB/T 2542 (2012). "Test methods for wall bricks," Standardization Administration of China, Beijing, China.
- GB/T 50129 (2011). "Standard for test method of basic mechanics properties of masonry," Standardization Administration of China, Beijing, China.
- He, J. X., Wang, J., and Yang, Q. S. (2017). "Mechanical property of column footing joint in traditional wooden structure by quasi-static test," *Journal of Building Structures* 38(08), 141-149. DOI: 10.14006/j.jzjgxb.2017.08.015
- He, Y. H., Ding, Y. W., Mohrmann, S., and Wang, Z. (2022). "Experimental and finite element method study on dynamic characteristics of beam-column glulam frame structure," *Advances in Structural Engineering* 25(13), 2738-2753. DOI: 10.1177/13694332221107577
- Hu, W. G., and Liu, N. (2020). "Numerical and optimal study on bending moment capacity and stiffness of mortise-and-tenon joint for wood products," *Forests* 11(5), article 501. DOI: 10.3390/f11050501
- Huan, J. H., Ma, D. H., Guo, X. D., and Xu, S. (2019). "Experimental study of aseismic behaviors of flexural tenon joint through tenon joint and dovetail joint reinforced with flat steel devices," *Journal of Beijing University of Technology* 45(8), 763-771. DOI: 10.11936/bjutxb2018010012

- Jacklin, B. R., EI Damatty, A. A., and Dessouki, A. A. (2014). "Finite-element modeling of a light-framed wood roof structure," *Wind and Structures* 19(6), 603-621. DOI: 10.12989/was.2014.19.6.603
- Jin, Y. C., Su, H. X., Pan, W., He, Y. C., Du, J. W., and Fu, G. P. (2022). "Experimental research on seismic performance and reinforcement comparison of mortise tenon joints in timber structures," *Journal of Civil and Environmental Engineering* 44(02), 138-147. (in Chinese). DOI: 10.11835/j.issn.2096-6717.2021.095
- JGJ/T 101 (2015). "Specification for seismic test of buildings," China Architecture and Building Press, Beijing, China.
- Liang, S. C. (2016). *Qing Ministry of Works: Examples of Engineering Practices*, Tsinghua University Press, Beijing, China.
- Liu, D. K. (2001a). "Roof loads of Chinese timber buildings: First volume," *Traditional Chinese Architecture and Gardens* 3, 58-64.
- Liu, D. K. (2001b). "Roof loads of Chinese timber buildings: second volume," *Traditional Chinese Architecture and Gardens* 4, 56-63.
- Ma, E. N., and Zhao, G. J. (2012). *Special Topics on Wood Physics*, China Forestry Publishing House, Beijing, China.
- Ma, L. L., Xue, J. Y., and Zhang, X. C. (2023). "Seismic performance evaluation of damaged ancient timber structures with looseness mortise-tenon joints," *International Journal of Architectural Heritage* 17(12), 2054-2068. DOI: 10.1080/15583058.2022.2097033
- Meng, X. J, Li, T. Y., Wang, Z. H., and Liu, H. (2022). "Numerical simulation and experimental verification of the hysteretic behavior of song style timber frame," *Journal of Taiyuan University of Technology* 53(4), 772-778. DOI: 10.16355/j.cnki.issn1007-9432tyut.2022.04.024
- Sun, Z. S., Xiang, P., Jia, L. J., and Zhang, R. (2022). "Seismic response and kinematic mechanisms of single-story pavilion-type timber frame based on shaking table test," *Structures* 45, 1701-1716. DOI: 10.1016/j.istruc.2022.10.016
- Tian, Y. F. (2013). *Knowledge Manual of Chinese Ancient Architecture*, Architecture & Building Press, Beijing, China.
- Tu, L. H. (2021). Experimental Study of Traditional Chuan-Dou Frames with Infill Under In-plane Cyclic Load, Master's Thesis, Southeast University, Jiangsu, China.
- Vieux-Champagne, F., Sieffert, Y., Grange, S., Belinga Nko'ol, C., Bertrand, E., Duccini, J. C., Faye, C., and Daudeville, L. (2017). "Experimental analysis of a shake table test of timber-framed structures with stone and earth infill," *Earthquake Spectra* 33(3), 1075-1100. DOI: 10.1193/010516eqs002m
- Wang, J., He, J. X., Yang, Q. S., and Yang, N. (2018). "Study on mechanical behaviors of column foot joint in traditional timber structure," *Structural Engineering and Mechanics* 66(1), 1-14. DOI: 10.12989/sem.2018.66.1.001
- Xie, Q. F., Zhang, L. P., Li, S., Zhou, W. J., and Wang, L. (2018). "Cyclic behavior of Chinese ancient wooden frame with mortise—tenon joints: Friction constitutive model and finite element modelling," *Journal of Wood Science* 64(1), 40-51. DOI: 10.1007/s10086-017-1669-5
- Xue, J. Y, Song, D. J., and Wu, C. W. (2023). "Precise finite element analysis of full-scale straight-tenon joints in ancient timber buildings," *International Journal of Architectural Heritage* 17(7), 1137-1152. DOI: 10.1080/15583058.2021.2017073

- Xue, J. Y, Xu, D., and Dai, W. Q. (2019). "Experimental study and numerical simulation analysis on seismic performance of continuous tenon joint in column-and-tie timber structure," *China Civil Engineering Journal* 52(11), 56-65. DOI: 10.15951/j.tmgcxb.2019.11.006
- Xue, J. Y., Xu, D., and Guo, R. (2020). "Shaking table tests and contrastive analysis for column-and-tie wooden buildings with and without infills," *Journal of Vibration and Shock* 39(13), 184-192+237. DOI: 10.13465/j.cnki.jvs.2020.13.027
- Yang, Q. S., Liu, K., Yu, P., and Law, S. S. (2024). "The analytical lateral load resisting performances of a bracket set frame in a traditional Chinese timber structure," *Structures* 61, article 106128. DOI: 10.1016/j.istruc.2024.106128
- Yeo, Y. S., Hsu, F. M., Komatsu K., Chung, L. Y., and Chang, S. W. (2016). "Shaking table test of the Taiwanese traditional Dieh-Dou timber frame," *International Journal of Architectural Heritage* 10(5), 539-557. DOI: 10.1080/15583058.2015.1009574
- Yi, D. H., Fan, Y. Q., Pan, Y., and Yuan, J. C. (2023). "Seismic behavior of predamaged mortise-and-tenon joints reinforced using viscoelastic dampers," *Journal of Structural Engineering* 149(9), article 04023124. DOI: 10.1061/jsendh.steng-12395
- Yuan, J. L., Li, S. C, and Song, T. (2022). "Study on seismic damage characteristic and law of ancient timber frame buildings," *Earthquake Engineering and Engineering dynamics* 42(03), 22-33. DOI: 10.13197/j.eeed.2022.0303
- Yu, P., Yang, Q. S., Law, S. S., and Liu, K. (2022). "Seismic performances assessment of heritage timber frame based on energy dissipation," *Journal of Building Engineering* 56, article 104762. DOI: 10.1016/j.jobe.2022.104762
- Zhang, L., Liu, C., and Zhou, T. (2022). "Experimental study on mechanical properties of column foot of ancient timber structures Take the drum-shaped plinth as an example," *Structures* 40, 1002-1013. DOI: 10.1016/j.istruc.2022.04.032
- Zhang, T. X., and Hu, W. G. (2021). "Numerical study on effects of tenon sizes on withdrawal load capacity of mortise and tenon joint," *Wood Research* 66(2), 321-330. DOI: 10.37763/wr.1336-4561/66.2.321330
- Zhang, X. C, Qiu, Z. H., Wu, C. W., Ma, H., Huo, J., and Shi, M. X. (2023). "Seismic evaluation of a traditional Chinese palace-style timber structure," *Soil Dynamics and Earthquake Engineering* 169, article 107878. DOI: 10.1016/j.soildyn.2023.107878
- Zhao, X. B., Zhang, F. L., Xue, J. Y., and Ma, L. L. (2019). "Shaking table tests on seismic behavior of ancient timber structure reinforced with CFRP sheet," *Engineering Structure* 197, article 109405. DOI: 10.1016/j.engstruct.2019.109405
- Zhou, Y., and Lv, X. L. (2016). *Method and Technology for Shaking Table Model Test of Building Structures*, Science Press, Beijing, China.
- Zhu, Z. M. (2015). Experimental Research on Mechanical Properties of Timber Structural Members with Shrinkage Cracks in Historic Buildings, Master's Thesis, Southeast University, Jiangsu, China.

Article submitted: November 12, 2024; Peer review completed: March 15, 2025; Revised version received: April 10, 2025; Accepted: April 11, 2025; Published: April 21, 2025. DOI: 10.15376/biores.20.2.4304-4329